REVIEW ARTICLE

Atmospheric interactions of planetary bodies with the solar wind

Max K. Wallis
Department of Applied Maths and Astronomy, University College, Cardiff CF1 1XL, UK

W.-H. Ip
Max-Planck Institut für Aeronomie, D-4311 Katlenburg-Lindau 3, FRG

Orbiting spacecraft about Venus have revealed a partially penetrable boundary sheath with induced fields limiting solar wind effects on the atmosphere structure and evolution. Mars differs structurally, the explanation awaiting an orbiter mission such as the European Space Agency is considering. In weak comets gyro-radii exceed other scale lengths, while in active comets the gas and solar plasma couple over the largest scale, boundary sheaths being unimportant—as occurred during early rapid-outgassing phases of Venus and Mars.

WHILE the early flyby missions of Mariners 2, 4 and 5 identified probable bow shocks in the solar wind plasma and showed that Venus[1] and Mars[2,3] do not possess large magnetospheres, the data were too limited to distinguish unambiguously between magnetic perturbations intrinsic to the solar wind and perturbations generated by interaction with the planets. Interpretation has largely been based on the gas dynamic or magneto-hydrodynamic (MHD) model of single-fluid flow past an impenetrable obstacle[4], recently refined to cover arbitrary inclination of a convected, weak external magnetic field in three dimensions[5]. It took the Soviet Mars 4–5 orbiting spacecraft to begin to reveal the novel processes and complex physics involved, and NASA's current Pioneer Venus Orbiter with a wide complement of instruments to give a qualitative leap in our understanding.

Before Pioneer Venus, the major characteristics of the solar wind interaction as established by Venera 9 and 10 Orbiters together with flyby and landing craft were as follows[6]. Venus does not have an Earth-like magnetosphere, its magnetic field being largely or wholly the result of induction by the solar wind[7]. The bow shock shape and position are roughly as predicted by gas-dynamic models (standing-off ahead of the planet by 0.15–0.3 times its radius), although there were indications that it is weaker, sometimes closer and more variable than implied by gas dynamics[8]. Such peculiarities together with unusual plasma structures in the wake and lack of energetic particles emanating from the bow shock[9], led to early suspicions of an extended planetary exosphere contributing a few new ions to the plasma flow and causing some comet-like characteristics[10]. Inputs of plasma and energy from the solar wind into the dayside ionosphere as well as into the surprisingly hot and extensive nightside ionosphere had been hypothesized but not directly confirmed[11]. Viscous-like velocity profiles were observed to extend downstream from the terminator, with streaming plasma bending into the planet wake[12]. Such profiles are expected when ion gyro-radii are comparable to the ionosheath thickness[13], but planetary ions drawn out into a comet-like tail also provide a plausible explanation[10].

How far the Mars 2–5 probes revealed differences between the Mars and Venus interactions is still controversial and likely to remain so until a further Orbiter is sent to Mars. As at Venus, an ionosheath extending into the tail constitutes a gradual transition from shocked solar wind to slowly-moving planetary ions[14,15]. The velocity profiles on the flank resemble shearing flow rather the canonical gas-dynamic model with a tangential discontinuity[4]. If the transverse scale of some 1,000 km corresponds to gyro-radius, the heavy ions are inferred to be C^+, N^+ and/or O^+, but there are questions over the detector and close identification is still lacking. Unlike at Venus where the ionosheath converges rapidly into the tail and perhaps emits a rarefaction wave, the diverging martian sheath is relatively limited (0.5 radii at 3–4 radii downstream) and has a rarefied interior containing little inhomogeneous plasma[14,15]. However, the extensive tail region and the nightside ionsophere have been explored rather little. The Mars bow shock stands further ahead of the planetary surface (0.5 rather than 0.3 ± 0.07 radii, according to new and compatible fitting procedures[16]) and the sheath has a wider flaring angle (some 30° compared with 20°)[17,18]. The low ionosphere density, presence of suprathermal ions ahead of Mars and abnormally cool ions in the sheath, and deviations from the gas dynamic model led to an early challenge to the magnetosphere idea[19]. This was reinforced by a demonstration that the magnetic field direction is consistent with solar wind field 'draped' around the planet[20]. Unfortunately the Viking Lander failed to carry even a simple magnetometer to resolve the issue of intrinsic Martian magnetization.

Three extreme models of the solar wind–atmosphere interaction have been proposed[21,22], as shown in Fig. 1. In model *a*, a strong magnetic field is supposed to be induced in the ionosphere, whose pressure counterbalances the solar wind's dynamic pressure. The configuration can be termed a 'pseudo-magnetosphere' by analogy with the Earth's magnetosphere. In model *b*, the magnetic field is assumed to remain weak, while ionospheric pressure balances the solar wind. In model *c*, the solar wind is pictured as flowing steadily into the atmosphere, being continuously modified by ionizing interactions. The plasma is eventually absorbed, through recombinations in the lower ionosphere. While *c* is perhaps appropriate to comets, it was recognized[19] that the steeply increasing density in the Mars

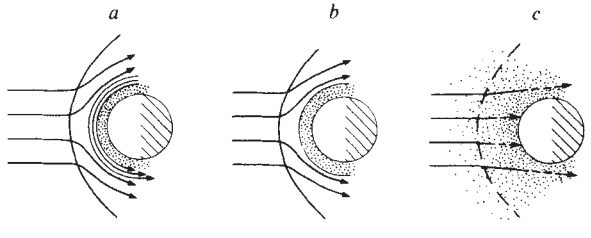

Fig. 1 Interaction models: the solar wind may be held off: *a*, by magnetic pressure; *b*, by ionospheric pressure; or *c*, partially absorbed.

0028-0836/82/280229—06$01.00

and Venus atmospheres and their small amounts of H and He render invalid the absorption plus weak shock model. However, the need to take into account the comet-like plasma interaction with neutral atmosphere still remained[19,22].

Venus interaction

The Pioneer Venus Orbiter marks a new stage in investigations of the atmosphere interaction with the solar wind, in giving us far greater detail over an extensive region of the planet for a prolonged period. Special journal issues assemble many of the experimental results[23]. Pioneer Venus established that the bow shock is indeed different from the Earth's, being weaker and closer to the obstacle[24], and probably departing from cylindrical symmetry[25,26]. Its position is insensitive to solar wind parameters and its limbs do not approach the Mach cone angle[27]. The shock structure is more diffuse, and is associated with enhanced plasma waves at 5 and 30 kHz, presumed due to planetary ions and consequent collective oscillations[28]. Pioneer Venus Orbiter data confirmed the induction concept[7], showing that currents and fields are induced within the ionosheath so as generally to exclude solar wind plasma and field[29], this sheath transition being a few tens of kilometres thick, at an altitude of typically 350 km at the nose increasing to 1,000 km at the terminator[30,31]. Figure 2*a* shows plasma and magnetic parameters along an orbit through the sheath into a low-field region

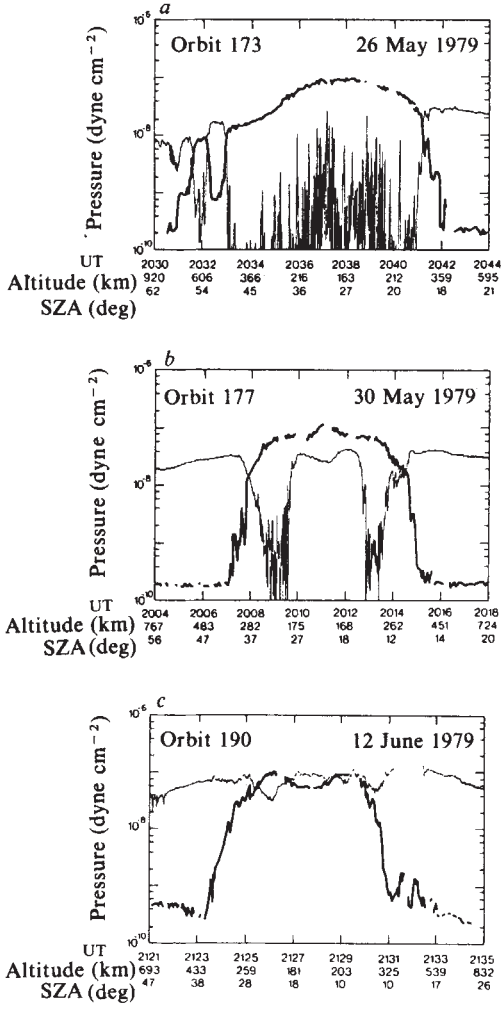

Fig. 2 Profiles from Pioneer Venus Orbiter[32] of magnetic (thin lines) and plasma (thick lines) pressures near periapsis, assuming electron temperature equal to that of the ions: *a*, the 'field-free' ionosphere with sporadic 'flux rope' enhancements; *b* and *c* magnetized ionosphere configurations. Note that the two pressures tend to have anti-correlated fluctuations. Probably $T_e = 2$–$3T_i$, so the plasma pressure could be larger than shown here[25,26].

and out again[32]. Note, however, the spiked enhancements of magnetic field outside the ionosphere, which correspond to twisted 'flux-rope' structures that occupy some 5% of the volume traversed[33]. The peak fields in the sheath of a few times 10^{-4} G exert the main pressure counterbalancing the solar wind, while the plasma pressure contributes some 20–30%. During periods of enhanced solar wind, the observations[32] stood in strong contrast (Fig. 2*b*, *c*). Apparently the ionosphere responds diamagnetically, resisting compression through electromagnetic induction of currents and a strong ionospheric field. This is understandable if the main induced field adjusts to solar wind changes with a finite delay time of 30 min or less[6], consistent with a conductivity of 1–2 S m^{-1} and so similar to estimates from gas–plasma collision rates[18]. At quiet times the field structure outside the sheath generally corresponds to solar wind field lines draped around the planet, with a corresponding ionospheric current system[34], but there seem to be connections to the ionospheric field and some interchange of ionospheric and solar wind plasma. Various possibilities have been identified: energetic solar wind may enter the dayside ionosphere along the twisted flux ropes of enhanced field[29,31], and some ionosheath solar wind may flow along field lines penetrating the nightside ionosphere, though flow from the upper dayside ionosphere seems to be the major ion source[35]. Fluctuating magnetic fields permit a fraction of the solar wind protons to diffuse into the terminator region[36], but dissipation of the induced currents is favoured for an external energy source on the dayside[29]. Figure 3 illustrates the large scale structure[6,34] and indicates the general plasma characteristics. Non-steady behaviour of the flow is important, perhaps dominant. Clouds of plasma appear to be stripped off the ionosphere in response to increases in the solar wind dynamic pressure[30,31]: these clouds could be the source of O^+ ions convected far downstream.

On the other hand, ionospheric chemistry implies that a weak suprathermal atomic O component of some 10^4 atoms cm^{-3} extends far out in the exosphere, to 3,000–5,000 km altitude[37]. When ionized in the solar wind, the oxygen constitutes additions of mass to the flow[38], it has been hypothesized, causing sheared velocity profiles and an apparently blunter obstacle. This magnetospheric rather than spherical-ionospheric shape has been modelled with an unphysically hot ionosphere[4,5]. Moreover, the new ions' gyro-radii of around 1,000 km exceed the ionosheath and ionosphere scales, so some of them should precipitate into the ionosphere and appear comparable with the energetic O^+ associated with substorms on Earth[38–40]. The dependence of precipitation on magnetic field direction could explain the observed shock asymmetry[8,25]. The relative importance of continuous sweeping up of new ions compared with detachment of ionosphere clouds is still unclear. Whichever the case, the general conclusion from Pioneer observations is that the interaction with Venus is less influenced by the degree of absorption of plasma than by planetary ions injected into the flow—influenced by comet-like sources of plasma rather than 'sinks'[41].

Mars interaction

Despite the many similarities indicated above, Mars does seem to differ significantly from Venus in its more distant bow shock, its wider-flaring, open ionotail[14,15], but a less extensive ionosphere on the planet flanks[18]. The magnetometer and electron-probe experimenters argue[17] that these differences imply a magnetic field intrinsic to Mars of dipole moment 2.5×10^{22} G cm^3. Independent examination of the published magnetic data has caused Russell[20] to dispute this: he set the dipole moment smaller by at least a factor 10 and argued that the magnetic field direction generally agrees with solar wind fields 'draped' over the ionosphere plus induced fields in the ionomagnetosheath. The larger value gives just enough magnetic pressure to hold off the quiet-time solar wind above the planet atmosphere—but not enough to withstand enhanced solar wind fluxes. A dynamic Venus-like interaction, with most of the field

Table 1 Solar wind parameters based on ref. 14 and derived interaction length scales (equation (3))

	AU	P_{stag}	Mach no.	Magnetic **B** (nT)	Spiral angle	$4\pi Q$ (s^{-1})	Length scales (km) R_B	R_{coll}	R_*	R_i
Venus	0.72	5.0	6.6	10	36°	10^{27}	6,050	—	6,410	2,000
Mars	1.52	1.1	7.9	3.3	57°	10^{27}	3,500	—	3,800	3,000
Comet Encke	1.0	2.5	7.2	6	45°	10^{27}	1	30	1,000	2,500
Comet Halley						10^{29}	3	3,000	10^5	2,500

Units of the ram pressure P_{stag} are 10^{-8} dyn cm^{-2}. Comets Encke and Halley are taken as typical examples of weak and active comets respectively at 1 AU, but all their parameters change with heliocentric distance.

being induced, is implied during periods of enhancements if not also during quiet conditions.

An intermediate stance on the dipole strength is taken by Intriligator and Smith[42], on the basis of the magnetic pressure necessary to supplement the plasma pressure of a model ionosphere. Figure 4*a* shows their magnetosphere model for a dipole moment 8×10^{21} G cm^3 (10^{-4} times the Earth's, giving an equatorial surface field of 21 nT), comprising two novel features: (1) the polar caps cover a significant portion of the planet's surface, and (2) the nightside atmosphere is directly connected to a tailward plasma-sheet. Planetwards convection of wake plasma at all longitudes is expected[43,44] (Fig. 4*b*) because the solar wind-induced electric field ($-\mathbf{U}_{SW}\times\mathbf{B}_{SW}\sim$ 1 kV across the diameter) is an order of magnitude larger than a co-rotation electric field at the magnetopause ($R_{MP}\boldsymbol{\Omega}\times\mathbf{B}_{MP}$). Ion–atmosphere collisions define a lower limit for the penetration of such convected plasma flow. Although the large polar caps appear open to the solar wind (Fig. 4*a*), it is possible that induction acts on the Venus pattern so as generally to impede penetration into the ionosphere. On this model the Mars interaction would be sensitive to the solar wind field orientation: because of the tendency to 'field reconnection', the front-side magnetosphere would tend like at Earth to be unstable when the solar wind and planetary fields are anti-parallel, but be relatively stable when parallel.

Alternative explanations have been proposed for the Mars shock and ionosheath lying further out than for Venus[18,45] (Fig. 2). Its exosphere has different composition and is more extensive, its ionosphere has higher conductivity, the planet is a relatively rapid rotator, and the solar wind β (ratio of flow to magnetic energy) is smaller at Mars. The latter two points are not supported as explanations by scaling laws[42,43], collisional conductivities are lower at Mars rather than higher[18], and in the light of Pioneer Venus observations, the exospheric explanation looks the most promising. The suprathermal O input from O_2^+ recombination is comparable on the two planets[45] but the martian exosphere is more extensive because of lower gravity. Suprathermal atomic N from various chemical processes provides an additional exospheric component of both escaping and bound gas[46].

Comets

Both Mars and Venus are believed to have lost much of their primitive atmospheres during their evolution. Instead of provoking minor modifications to the solar wind flow, the abundant escaping exosphere at earlier epochs would have given them the character of comets. It is now understood that ions created in the extensive comas of larger comets dominate the oncoming solar wind[47]. Virtually all the solar protons that penetrate to a few times 10^4 km are neutralized through charge exchange[48]. Theory indicates that new cometary ions would be picked-up by large scale **E** and **B** fields or by fluctuating small scale fields, the latter resulting from plasma instabilities driven by the relatively streaming ion beams[49,50].

In comets where new ions have relatively small gyro-radii, their primary effect appears as 'mass loading' giving deceleration of the solar wind flow[47,51]. In a supersonic one-dimensional flow, the maximum proportional mass addition is $(\gamma^2-1)^{-1}$. For a source flow of strength Q molecules s^{-1} sr^{-1} at speed V interacting through charge exchange with cross-section σ_{ex}, the deceleration radius is given[52] by

$$(\gamma^2-1)^{-1}=A_i\int_{R_*}^{\infty}\sigma_{ex}\frac{Q}{V}\frac{dR}{R^2}\quad\text{or}\quad R_*=(\gamma^2-1)A_i\sigma_{ex}\frac{Q}{V} \tag{1}$$

taking the density to follow an inverse square law. (Models in which the density drops off much more steeply with R, due to radiation pressure[53] or to plasma drag[54], are unrealistic.) With mean atomic weight $A_i\sim20$ and $Q/V\sim10^{23}$ cm^{-1}, this gives an estimate of $R_*=10^5$ km for a good-sized comet such as Halley. Allowance for photo-ionization and more readily ionized components such as OH gives a slightly larger estimate for R_*, but because photo-ionization makes a minor contribution the value depends little on solar fluxes[52]. This parameter R_* is the scale standoff distance for the cometary bow shock, weakened because the plasma ahead of it is energized through the pick-up processes: on model calculations its Mach number is ~2 (refs 51, 55, 56), even weaker than that observed at Venus. If instability-associated processes are sufficiently dissipative, the cometary shock as a region of enhanced dissipation may even be absent.

The scale for plasma–gas coupling and limit of the collision-dominated coma

$$R_{coll}=\sigma_{coll}Q/V \tag{2}$$

is in all cases smaller than R_* by more than a factor 10 because the cross-section factors are comparable. The shock stand-off distance R_* is thus far greater than (and unrelated to) the effective obstacle size, unlike normal hypersonic flow past an obstacle such as a magnetosphere[51]. The flow regions deduced are depicted in Fig. 5*a*.

Such a novel shock has not yet been investigated in practice and several points in the argument need experimental

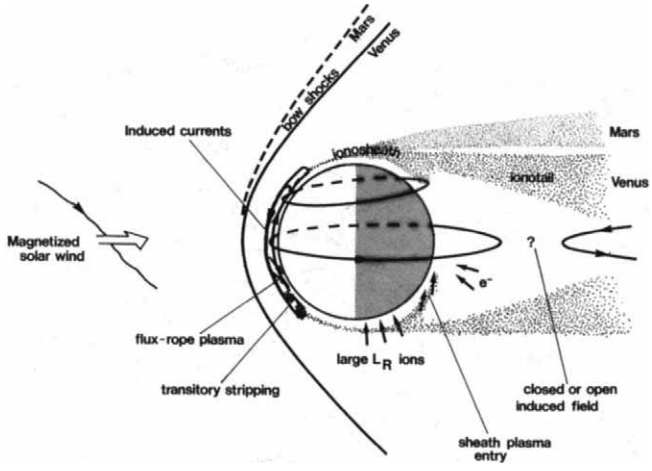

Fig. 3 Schematic of the Venus interaction with the solar wind, showing large-scale induced current and magnetic structure, and indicating various mechanisms for plasma interchange identified by Pioneer Venus. Representative positions of the wider bow shock and ionosheath at Mars as detected by the Mars Orbiters are shown in comparison (scaled to the planet radius).

verification. The net result of the ion pick-up interaction can differ significantly from Venus in the way the energy of the decelerated solar wind is distributed between plasma species and fields. A weak resistive shock causes little heating of the ions and electrons (order 10 eV per particle) while pick-up in a transverse field can give up to keV per nucleon to cometary ions in the outer coma[19]. In practice the fraction of energy going to the protons and electrons is probably not negligible but still relatively small.

Cometary ions picked up in the far unperturbed solar wind have gyro-velocities up to the solar wind speed and so gyro-radii R_i of the order of 10^4 km. Thus for weaker comets such as ncke with[57] peak $Q/V \simeq 10^{21}$ H_2O molecules cm^{-1}, equation (1) gives $R_* < R_i$. However, R_* still exceeds the obstacle size R_{coll} from equation (2) and the body radius R_B (comet nucleus radius 1–5 km). The collisionless shock thickness R_s is a few solar wind proton gyro-radii, that is $R_s \simeq (0.1\text{–}1)R_i$. At comet Encke's peak with $R_* \simeq R_i$, the fluid description with ion pick-up is scarcely valid, and further from the Sun where Q drops by a factor of 10–100, the scale parameters characterizing a weak comet are ordered as

$$R_i \geq R_s > R_* > R_{coll}, R_B \quad (3)$$

Comet Halley outside 3 AU is similarly weak. The cometary ions do not see the tiny comet nucleus or collisional atsmophere, and the potential disturbance scale R_* is smaller than the shock thickness. The dominant physical process is still interaction with large gyro-radius cometary ions, but as individual charged particles rather than a quasi-fluid. Laboratory experiments[58] also have $R_i \gg R_* > R_B$, so they simulate weak comets (but not typical ones). For Venus, Mars and large satellites such as the Moon, $R_B \geq R_i$ unlike relationship (3), so special ionosheath or boundary structures are plausible for them but not expected for comets.

Dust grains up to 30 μm radius can be blown off during comet Encke's maximal outgassing (rate 10^{26} s^{-1} sr^{-1}), while at lower rates, spin of the nucleus or electrostatic forces[59] may help expel the grains. Micrometre-sized grains attain terminal speeds

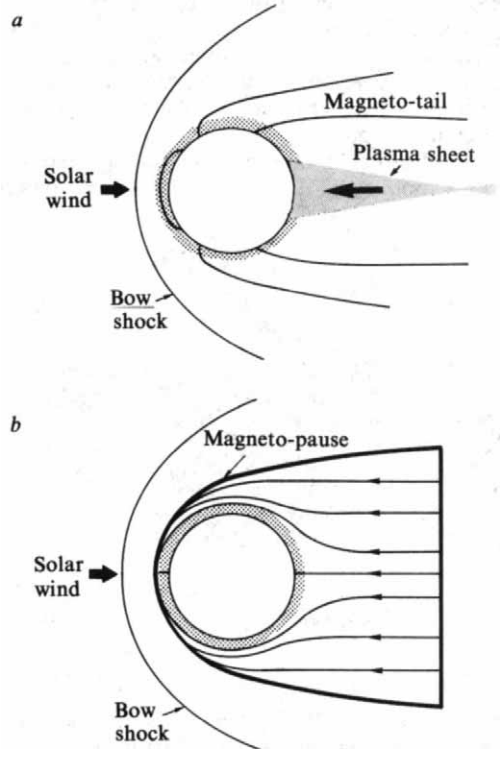

Fig. 4 The hybrid martian magnetosphere for a marginally important intrinsic planetary field (after ref. 42) in planes normal (*a*) and parallel (*b*) to the dipole.

of 10 m s^{-1}, so are blown tailwards by radiation pressure on the 100-km scale[60] (since speeds $\sim Q^{1/2}$, the scale is of order $0.1R_*$ for all Q at 1 AU, of order R_* at 3 AU). The dust coma and tail consist of individual grains, with only the finest ones ($a < 0.03$ μm) which see little radiation pressure[60] able to penetrate far laterally. Such grains being charged suffer perturbations from the solar wind fields as well as sputtering by solar protons, but on far larger scale lengths. Their own effect on the plasma flow is negligible, proton collisions with dust grains being much less frequent than with neutral gas, supposing gas and sub-micrometre dust production at similar rates and a velocity ratio of order 100. Thus for a weak and dusty comet we derive the situation sketched in Fig. 5*b*, with the dust and plasma essentially uncoupled. Some long-lived large (1 mm–1 cm) grains[61] can also extend past the main dust envelope (Fig. 5*b*), possibly because the nucleus spin is rapid enough to eject grains against gravity.

The famous plasma envelopes are probably distinctive of large comets, being dependent on small gyro-radius. The CO^+-rich Comet Morehouse of 1908 showed a series of plasma envelopes forming at a distance of $1\text{–}3 \times 10^5$ km ahead of the nucleus[62,63]. The time scale for formation was typically 1 h or so; as each envelope grew, it seemed to recede towards the nucleus. In the course of contraction, the structures became sharper and sometimes connections could be traced between these envelopes and the symmetric ion rays in the tail. Morphologically speaking, these symmetric tail rays may reflect inhomogeneous ion production, with ions expanding along field lines, or the collapsing of denser ion shells extending from the envelopes, like a folding umbrella[64]. Either way these features are indicative of the non-stationary and inhomogeneous nature of the solar wind–comet interaction.

The region inside R_{coll} (equation (2)) where the ions and electrons must be closely coupled to the outflowing cometary gas, is termed the cometary ionosphere (Fig. 5*a*). It differs from a planet's ionosphere in that the dynamical expansion interferes with photochemical equilibrium, the composition changing with radius R. However, computations[65,66] show that the overall ion density and stagnation pressure are not far from the photochemical law: $p_{stag} = p_e + p_i + \rho_i V_i^2 \propto R^{-k}$, $k \simeq 1$. The transition from the ionosphere to the plasma inflow (solar wind plus picked-up cometary ions) is still a matter of controversy[48,54]. Downstream of the shock, collisional cooling processes compete with ion pick-up deceleration, but the pressure in the subsonic region is expected to stay not much below the solar wind stagnation pressure $P_{stag} = p_\infty + \rho_\infty U^2 + B^2/8\pi$ (refs 51, 56). The ionospheric p_{stag} might exceed this if heating is high or ionization processes are enhanced; but probably collisional cooling and recombination keep $p_{stag}(R_{coll}) < P_{stag}$ by more than a factor of 10 (ref. 48). In this situation, the stagnation flow occurs well into the collisional region and interaction with the neutral gas also dominates the incoming plasma flow. Inclusion of magnetic field whose pressure is limited to around P_{stag} would not change the situation qualitatively[56].

Among cometary ions, CO^+ usually has the strongest optical emissions. CH^+, N_2^+, CO_2^+ and H_2O^+ are also evident around 10^4 km from the nucleus and extending into the tail[67]; H^+, C^+, O^+ and OH^+ should be more numerous and extensive, but still await direct detection. Much information is contained in the morphology of the ion tails long observed from Earth. The generation and gradual folding of the CO^+ ion rays onto the central tail axis are doubtless indicative of magnetic field 'draping'[68], the sheared velocity field of the plasma flow, a dynamic solar wind interaction and/or inhomogeneous ion production mechanisms[69,70]. Large-scale wave structures seen in some tails are well modelled as a non-linearly stabilized Kelvin–Helmholtz helical mode[71].

By analogy with the magnetotails of Earth and Venus, the presence of a current sheet (or sheets) and reconnection processes can be expected[72]. Ionization through auroral-type electrons and plasma acceleration through Lorentz forces have been hypothesized[72–74]. Accelerating potentials presumably depend

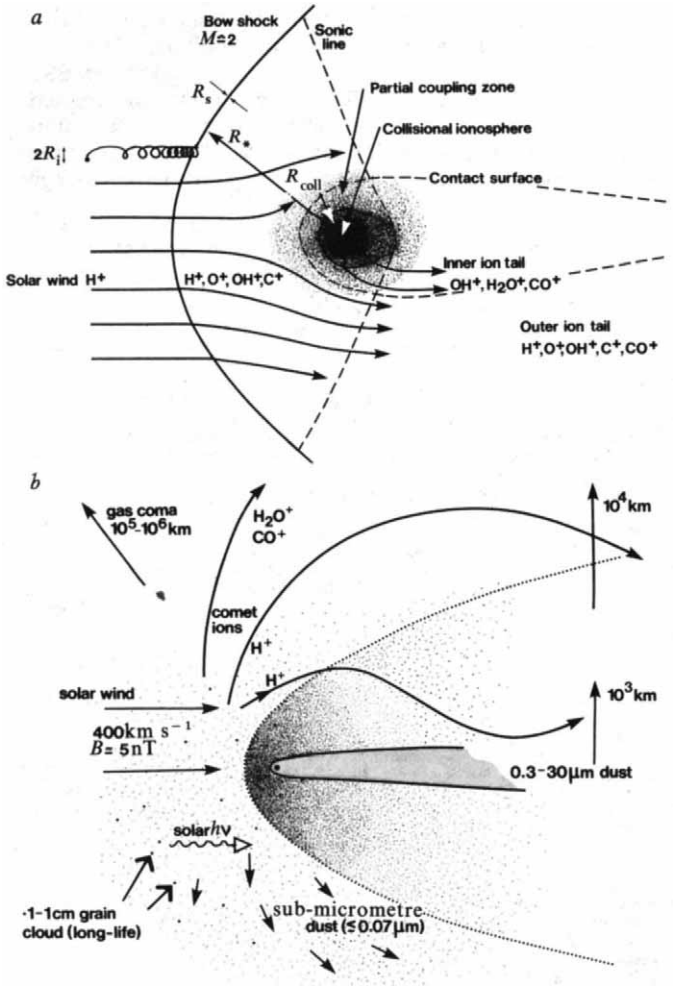

Fig. 5 Flow regions and scales: *a*, in a larger, gassy comet with streamlines indicating the mean plasma flow, though individual ons may undergo chemical reactions before progressing far along them; *b*, in a weak dusty comet where ion gyroscales and molecule free paths are large. Micrometre-sized dust released with the gas behaves as individual grains in a largely undisturbed solar wind, whose low speeds mean that radiation pressure blows them back into a narrow tail. Long-lived grains and sub-micrometre dust, (small enough to avoid most photons) populate the outer dust coma.

on the permeability of the ionosheath and the potential of the motional electric field across the tail $\phi = UBd/c$ for the tail diameter d. Although the values of d for comets and Venus are more than an order of magnitude smaller than the Earth's, the permeability of thick cometary ionosheaths is probably less than the unstable Venus one, so accelerating potentials would be intermediate at several kilovolts. Mean fields in the comet tail have strength similar to the interplanetary B_0 and as at Venus can have dynamically a near-passive role. However, higher fields up to 50 nT corresponding to p_{stag} should exist in the stagnation region[29] and perhaps in inhomogeneous structures analogous to the Venus flux ropes[33].

Conclusions

A realistic model of the Mars and Venus interactions with the solar wind must contain elements from each of the extreme cases depicted in Fig. 1. The induced field and ionospheric plasma in combination counterbalance the solar wind, while neutral atmosphere outside the ionosphere interacts with the plasma. Additional elements demonstrated by Pioneer Venus are the non-stationary nature and a degree of permeability of the ionopause to plasma and small scale fields[30,31]. The ionosphere's response, still largely unknown, is presumably characterized by the strong variability revealed in the ionosheath thickness and position[30,31], in some ways analogous to cometary 'envelopes' and tail rays. The Mars situation may be complicated by a small planetary field, making it a hybrid of Mercury and Venus[42] and more unstable when the interplanetary field is anti-parallel. Such a field is too weak to hold off the solar wind at all times[18], so Mars constitutes a novel transitional case of solar wind interaction. The planet's high rotation rate and atmosphere transparency imply that latitudinal variations and ionospheric winds will be much less severe than at Venus. One lesson from Pioneer Venus is that plasma analysers covering the full mass–energy range from solar wind protons to ionospheric O^+, O^{2+}, CO_2^+ at thermal energies are clearly needed. A second is that high time resolution is essential and dual spacecraft studies greatly advantageous for analysing the moving structures.

From a scientific point of view, Pioneer Venus opened up a whole spectrum of interesting physics: a Mars orbiter mission as is under study by ESA is the natural sequel. Not only are we now clearer on what to expect, we also know the kind of instrumentation needed. The novel phenomena discovered by the Pioneer Orbiter as well as the striking differences confirmed in the plasma and atmospheric environments of the two planets require systematic study. Specification of the non-thermal planetary ions should reveal the acceleration processes: a combination of ion sensors with magnetometer and plasma wave detectors would distinguish the role of adiabatic and plasma-turbulent pick-up of ions from the outer exosphere. The important non-thermal neutrals resulting from charge exchange, dissociative recombination, solar wind sputtering and energetic ion precipitation are difficult to measure, but new instruments are under development. Direct exploration of the hot corona of suprathermal neutrals (barely detected by the Venera and Pioneer spacecraft) may thus be feasible.

The current atmosphere loss from Venus and Mars is determined not by thermal processes but by the solar wind interaction and ionospheric chemistry. Calculations of the Venus H-loss consistent with explanations for the extensive corona observed in H Lyα, range from 8×10^6 cm^{-2} s^{-1} up to 1×10^8 cm^{-2} s^{-1}, the latter for a maximum hypothetical H_2 atmospheric component[75,76]. Ionization of the suprathermal O above the ionopause[37,77,78] averages 1×10^7 cm^{-2} s^{-1} (mean ionopause heights of ref. 30) interaction with the solar plasma may return 25% to the planet and sweep the remainder into the tail (this flux is a factor 2–3 smaller than that estimated for O^+ structures convected into the wake[31]). It is not yet clear whether the H and O losses are in the ratio of H_2O, as indicated for Mars, or whether atmospheric O is absorbed in Venus surface rocks.

The equivalent planetary interaction parameters to those for weak and active comets are estimated as in Table 1. The plasma–atmosphere coupling radius R_* for Venus and Mars is determined not strictly by equation (1) but as the radius at which a tangential solar plasma flow suffers substantial deceleration[22]. That the O^+ gyroradii are large undermines such a concept, but with the steeply-varying exosphere density the uncertainty in R_* is small. Comparison of the radial scales in Table 1 shows the different ordering of R_i and R_* for the two comets, as well as their similarity to the body size R_B for the planets; the latter implies that boundary layer and finite gyroradius effects are significant.

It is known[79] that Mars through its history has lost much of its N and O: the 64% enrichment of the heavy ^{15}N isotope recorded by Viking[79] is explained by chemical processes producing atoms above the escape speed. In contrast the negligible enrichment of the ^{18}O isotope suggests that solar wind pickup with no isotope preference has overwhelmingly dominated the O-loss processes. At earlier evolutionary epochs Mars and Venus both had far more H_2O and loss rates were doubtless far higher[80,81]. The 'runaway greenhouse' effect is invoked[80] to explain Venus loss rates 10^6 times higher than present. This implies a total loss $4\pi Q \sim 3\times10^{31}$ H_2O s^{-1}, a factor 10^2–10^3 larger than the model for comet Halley (Table 1). Equation (1)

implies an interaction scale with the solar wind of $R_* = 10^7$–10^8 km, a truly giant comet. (This extrapolated scale should not be taken literally, as photoionization and radiation pressure restrict the extension into space of the neutral gases.)

Clearly, intermediate stages during Mars and Venus atmosphere loss would also be cometary. Justification for the Giotto mission to Comet Halley and for a new Mars Orbiter mission lies not merely in winning understanding of their present interactions with the solar wind, but also in achieving realistic modelling of the planets' past and future evolution.

An initial version of this review was presented at the ESF Workshop on Planetology at Strasbourg (1980) and revised while M.K.W. was a visiting scientist at the Max-Planck Institut für Aeronomie, Lindau, and holding an SRC Fellowship at the Mullard Space Science Laboratory of University College London.

1. Bridge, H. S. *et al. Science* **158,** 1669–1673 (1967).
2. Smith, E. J., Davis, L., Coleman, P. J. & Jones, D. E. *Science* **149,** 1241–1242 (1965).
3. Lazarus, A. J., Bridge, H. S., Davis, J. M. & Snyder, C. W. *Space Res.* **7,** 1296 (1967).
4. Spreiter, J. R., Summers, A. L. & Rizzi, A. W. *Planet. Space Sci.* **18,** 1281–1290 (1970).
5. Spreiter, J. R. & Stahara, S. S. *J. geophys. Res.* **85,** 7715–7738 (1980).
6. Breus, T. K. *Space Sci. Rev.* **23,** 253–275 (1979).
7. Eroshenko, E. G. *Kosmich. Issled.* **17,** 93–105 [*Cosmic Res.* **17,** 77–87] (1979).
8. Romanov, S. A., Smirnov, V. N. & Vaĭsberg, O. L., *Kosmich. Issled.* **16,** 746–756 [*Cosmic Res.* **16,** 603–611] (1978).
9. Simpson, J. A., Eraker, J. H., Lamport, J. E. & Walpole, P. H. *Science* **183,** 1318–1321 (1974).
10. Wallis, M. K. *Cosmic Electrodyn.* **3,** 45–49 (1972); in *Cosmic Plasma Phys.* (ed. Schindler, K.) 137–140 (Plenum, New York, 1972).
11. Bauer, S. J. *et al., Space Sci. Rev.* **20,** 413–430 (1977).
12. Pérez-de-Tejada, H., Dryer, M. & Vaĭsberg, O. L. *J. geophys. Res.* **82,** 2837–2841 (1977).
13. Lipatov, A. S. *Kosmich. Issled.* **16,** 429–433 [*Cosmic Res.* **16,** 346–349] (1978).
14. Bogdanov, A. V. & Vaĭsberg, O. L. *J. geophys. Res.* **80,** 487–494 (1975).
15. Vaĭsberg, O. L., Bogdanov, A. V., Smirnov, V. N. & Romanov, S. A. *NASA SP-397,* 21–38 (1976).
16. Slavin, J. A. & Holzer, R. E. *J. geophys. Res.* **86,** 11401–11418 (1981).
17. Dolginov, Sh.Sh., Yeroshenko, Ye. G. & Zhuzgov, L. N. *J. geophys. Res.* **81,** 3353–3362 (1976).
18. Breus, T. K. & Gringauz, K. I. *Kosmich. Issled.* **18,** 587–599 [*Cosmic Res.* **18,** 426–437] (1980).
19. Wallis, M. K. *Geophys. J. R. astr. Soc.* **41,** 349–354 (1975).
20. Russell, C. T. *Geophys. Res. Lett.* **5,** 81–88 (1978).
21. Michel, F. C. *Rev. Geophys. Space Phys.* **9,** 427–435 (1971).
22. Wallis, M. K. *Solar Wind Three* (ed. Russell, C. T.) 421–427 (Institute of Geophysics UCLA, 1974).
23. *Science* **203** (February 1979); **205** (July 1979); *J. geophys. Res.* **85,** No. A13 (1980).
24. Russell, C. T., Elphic, R. C. & Slavin, J. A. *Nature* **282,** 815–816 (1979).
25. Smirnov, V. N., Vaĭsberg, O. L. & Intriligator, D. S. *J. geophys. Res.* **85,** 7651–7654 (1980).
26. Vaĭsberg, O. L., Intriligator, D. S. & Smirnov, V. N. *Kosmich. Issled.* **29,** 104–113 [*Cosmic Res.* **29,** 75–82] (1981).
27. Slavin, J. A. *et al., J. geophys. Res.* **85,** 7625–7641 (1980).
28. Scarf, F. L., Taylor, W. W. L., Russell, C. T. & Elphic, R. C. *J. geophys. Res.* **85,** 7599–7612 (1980).
29. Elphic, R. C., Russell, C. T., Slavin, J. A. & Brace, L. H. *J. geophys. Res.* **85,** 7679–7696 (1980).
30. Brace, L. H. *et al. J. geophys. Res.* **85,** 7663–7678 (1980).
31. Elphic, R. C., Russell, C. T., Luhmann, J. G., Scarf, F. L. & Brace, L. H. *J. geophys. Res.* **86,** 11430–11438 (1981).
32. Luhmann, J. G., Elphic, R. C., Russell, C. T., Mihalov, J. D. & Wolfe, J. H. *Geophys. Res. Lett.* **7,** 917–920 (1980).
33. Russell, C. T. & Elphic, R. C. *Nature* **279,** 616–618 (1979).
34. Luhmann, J. G., Elphic, R. C. & Brace, L. H. *J. geophys. Res.* **86,** 3509–3514 (1981).
35. Hoegy, W. R., Brace, L. H., Theis, R. F. & Mayr, H. G. *J. geophys. Res.* **85,** 7811–7816 (1980).
36. Gombosi, T. I., Cravens, T. E. & Nagy, A. F. *J. geophys. Res.* **85,** 7747–7753 (1980).
37. Wallis, M. K. *Planet. Space Sci.* **26,** 949–953 (1978); *Q. Jl R. astr. Soc.* **20,** 437–438 (1979).
38. Cloutier, P. A., Daniell, R. E. & Butler, D. M. *Planet. Space Sci.* **22,** 967–990 (1974).
39. Torr, M. R. & Torr, D. G. *Geophys. Res. Lett.* **6,** 700–702 (1979).
40. Wallis, M. K. *Geophys. Res. Lett.* **9,** 427–430.
41. Russell, C. T. *Geophys. Res. Lett.* **4,** 387–390 (1977).
42. Intriligator, D. S. & Smith, E. J. *J. geophys. Res.* **84,** 8427–8435 (1979).
43. Siscoe, G. L. in *Solar System Plasma Physics* (ed. Kennel, C. F. *et al.*) (North Holland, Amsterdam, 1978).
44. Bauer, S. J. & Hartle, R. E. *J. geophys. Res.* **78,** 3169–3171 (1973).
45. Vaĭsberg, O. L. *et al., Kosmich. Issled* **10,** 462–463 [*Cosmic Res.* **10,** 417–418] (1972).
46. Fox, J. L. & Dalgarno, A. *Planet. Space Sci.* **28,** 41–46 (1980).
47. Biermann, L., Brosowski, B. & Schmidt, H. U. *Solar Phys.* **1,** 254–284 (1967).
48. Wallis, M. K. & Ong, R. S. B. in *The Study of Comets* 856–876 (NASA SP-393 (1976).
49. Wallis, M. K. *Nature phys. Sci.* **233,** 23–25 (1971).
50. Hartle, R. E. & Wu, C. S. *J. geophys. Res.* **78,** 5802 (1973).
51. Wallis, M. K. *Planet. Space Sci.* **21,** 1647–1660 (1973).
52. Wallis, M. K. *Astr. Astrophys.* **29,** 29–36 (1973).
53. Beard, D. B. *Astrophys. J.* **245,** 743–752 (1981).
54. Houpis, H. L. F. & Mendis, D. A. *Astrophys. J.* **239,** 1107–1118 (1980).
55. Brosowski, B. & Wegmann, R. *Meth. Verf. mater. Phys.* **8,** 125–145 (1973).
56. Schmidt, H. U. & Wegmann, R. *Scientific and Experimental Aspects of the Giotto Mission,* 3–7 (ESA SP-169, 1981).
57. Keller, H. U. *Space Sci. Rev.* **18,** 641–684 (1976).
58. Podgorny, I. M., Dubinin, E. M., Potanin, Yu. N. & Shkolnikova, S. I. *Astrophys. Space Sci.* **61,** 369–374 (1979).
59. Mendis, D. A., Hill, J. R., Houpis, H. L. F. & Whipple, E. C. *Astrophys. J.* **249,** 787–797 (1981).
60. Burns, J. A., Lamy, P. L. & Soter, S. *Icarus* **40,** 1–48 (1979).
61. Sekanina, Z. & Shuster, H. E. *Astr. Astrophys.* **68,** 429–435 (1978).
62. Eddington, A. S. *Mon. Not. R. astr. Soc.* **70,** 442–458 (1910).
63. Lüst, Rh. *Z. Astrophys.* **65,** 236–250 (1967).
64. Marochnik, L. S. *Usp. Fiz. Nauk* **82,** 221–252 [*Soviet. Phys. Usp.* **7,** 80–100] (1964).
65. Ip, W.-H. *Astr. Astrophys.* **92,** 95–100 (1980).
66. Giguère, P. I. & Huebner, W. F. *Astrophys. J.* **238,** 753–762 (1980).
67. Wyckoff, S. & Wehninger, P. A. *Astrophys. J.* **204,** 604–615 (1976).
68. Alfvén, H. *Tellus* **9,** 92–96 (1957).
69. Wurm, K. in *The Moon Meteorites and Comets,* (eds Middlehurst, B. M. & Kuiper, G. P.) 573–617 (University of Chicago Press, 1963); *Icarus* **8,** 287–300 (1968).
70. Ness, N. F. & Donn, B. *Mem. Soc. Roy. Sci. Liège, ser.* 5, **12,** 141–144 (1966).
71. Ershkovich, A. I. *Space Sci. Rev.* **25,** 3–34 (1980).
72. Ip, W.-H. & Mendis, D. A. *Icarus* **26,** 457–461 (1976).
73. Mendis, D. A. *Moon and Planets* **18,** 361–369 (1978).
74. Ip, W.-H. *Planet. Space Sci.* **27,** 121–125 (1979).
75. Kumar, S., Hunten, D. M. & Broadfoot, A. L. *Planet. Space Sci.* **26,** 1063–1075 (1978).
76. Kumar, S., Hunten, D. M. & Taylor, H. A. *Geophys. Res. Lett.* **8,** 237–240 (1981).
77. Nagy, A. F., Cravens, T. E., Yee, J-H. & Stewart, A. F. I. *Geophys. Res. Lett.* **8,** 629–632 (1981).
78. Brace, L. H., Theis, R. F. & Hoegy, W. R. *Planet. Space Sci.* **30,** 29–37 (1982).
79. Nier, A. O. & McElroy, M. B. *J. geophys. Res.* **82,** 4341–4349 (1977).
80. Marov, M. Ya. *Fund. Cosmic Phys.* **5,** 1–46 (1979).
81. Pollack, J. L. & Yung, Y. L. *Ann. Rev. Earth planet. Sci.* **8,** 425–487 (1980).

ARTICLES

Geology and chemistry of hydrothermal deposits from active submarine volcano Loihi, Hawaii

Alexander Malahoff*, Gary M. McMurtry†, John C. Wiltshire‡ & Hsueh-Wen Yeh†

*National Ocean Survey–NOAA, Rockville, Maryland 20852, USA
†Hawaii Institute of Geophysics, and ‡Department of Oceanography, University of Hawaii, Honolulu, Hawaii 96822, USA

High-resolution bathymetric surveys, bottom photography and sample analyses show that Loihi Seamount at the southernmost extent of the Hawaiian 'hotspot' is an active, young submarine volcano that is probably the site of an emerging Hawaiian island. Hydrothermal deposits sampled from the active summit rift system were probably formed by precipitation from cooling vent fluids or during cooling and oxidation of high-temperature polymetallic sulphide assemblages. No exotic benthic fauna were found to be associated with the presently active hydrothermal vents mapped.

LOIHI Seamount is an active submarine volcano that marks the southernmost extent of the Hawaiian 'hotspot' and the probable site of an emerging Hawaiian island (Fig. 1). It is one of the two known active hotspot submarine volcanoes of the Pacific Ocean; the other is the relatively inaccessible Macdonald Seamount of the Austral Island Chain[1]. Although Loihi is ~50 km south-southwest of Kilauea caldera, it apparently is not volcanically associated with Kilauea's south-west rift zone[2].

0028-0836/82/280234—06$01.00